HTML ABSTRACT + LINKS

Characterization of a liquid-xenon-jet laser-plasma extreme-ultraviolet source

B. A. M. Hansson,[a] O. Hemberg, and H. M. Hertz
Biomedical & X-Ray Physics, Royal Institute of Technology/Albanova, SE-106 91 Stockholm, Sweden

M. Berglund,[b] H.-J. Choi, B. Jacobsson,[c] E. Janin, S. Mosesson, L. Rymell, J. Thoresen, and M. Wilner
former Innolite AB, Sweden c/o Biomedical and X-Ray Physics, Royal Institute of Technology/Albanova, SE-10691 Stockholm, Sweden

(Received 25 November 2003; accepted 29 March 2004; published online 24 May 2004)

A liquid-xenon-jet laser-plasma source for extreme-ultraviolet (EUV) and soft-x-ray generation has been characterized. Being a source candidate for EUV lithography (EUVL), we especially focus on parameters important for the integration of the source in EUVL systems. The deep-ultraviolet (DUV) out-of-band radiation ($\lambda = 120-400$ nm) was quantified, to within a factor of two, using a flying-circus tool together with a transmission-grating spectrograph resulting in a total DUV conversion efficiency (CE) of $\sim 0.33\%/2\pi$sr. The size and the shape of the xenon plasma was investigated using an in-band-only EUV microscope, based on a spherical Mo/Si multilayer mirror and a charge-coupled device detector. Scalability of the source size from 20–270 μm full width at half maximum was shown. The maximum repetition-rate sustainable by the liquid-xenon-jet target was simulated by a double-pulse experiment indicating feasibility of >17 kHz operation. The xenon-ion energy distribution from the plasma was determined in a time-of-flight experiment with a Faraday-cup detector showing the presence of multi-kilo-electron-volt ions. Sputtering of silicon witness plates exposed to the plasma was observed, while a xenon background of >1 mbar was shown to eliminate the sputtering. It is concluded that the source has potential to meet the requirements of future EUVL systems. © *2004 American Institute of Physics.*
[DOI: 10.1063/1.1755441]

I. INTRODUCTION

Laser plasmas based on inert-gas targets are attractive as negligible-debris extreme-ultraviolet (EUV) and soft-x-ray sources. An example is the xenon-liquid-jet laser plasma.[1,2] This article reports on the characterization of several important parameters of this source from a point of view of its applicability for full-scale EUV-lithography (EUVL) steppers.

EUVL[3] at $\lambda \sim 13.5$ nm is considered by many as the strongest candidate to succeed deep-ultraviolet (DUV) lithography for large-scale manufacturing of integrated circuits.[4] The EUV radiation source has, however, been identified[5] as the largest obstacle toward realization of EUVL since no source technology currently meets all the requirements for a production tool. Nonetheless, several source concepts, all based on hot plasmas, are under intense development.[6] These include electrically driven plasmas, e.g., *z*-pinch, plasma focus, capillary discharge, and hollow cathode discharge, as well as several laser-produced-plasma concepts.

Laser plasmas in general are not only applicable for EUVL[7] but are also potentially suitable as table-top sources of soft-x-ray and EUV radiation for applications such as proximity x-ray lithography,[8,9] x-ray microscopy,[10] and x-ray photoelectron spectroscopy.[11] The liquid-xenon-jet laser-plasma source[1,2] is an especially attractive source technology since it combines the advantages of the microscopic-liquid-jet target method[12,13] and an inert gas, high-*Z* target material.[14] The regenerative liquid-jet target allows for long-term high-repetition-rate operation at long distance from any source hardware, thereby minimizing thermal issues. Furthermore, the use of xenon as target material eliminates the creation of condensing or reactive target vapor associated with conventional target materials.

In the present article, we report on quantitative characterization of a liquid-xenon-jet laser-plasma source with respect to its applicability as an EUV source. Such accurate characterization is especially important since the source will eventually operate in an EUVL stepper, i.e., a complicated optical system. Thus, a system's perspective is necessary in order to optimize the performance of the full system and not only that of the source. Such a system analysis has resulted in a detailed list of source requirements commonly agreed upon by the major stepper companies.[15] In the present article, we report data on several important parameters of the liquid-xenon-jet source: non-EUV emission from the plasma, size and shape of the plasma, the repetition-rate limit of the source, and ionic emission from the plasma. Furthermore,

[a]Electronic mail: bjorn.hansson@biox.kth.se
[b]Current affiliation: Max-Lab, Lund University, Box 112, SE-221 00 Lund, Sweden.
[c]Current affiliation: Laser Physics and Quantum Optics, Royal Institute of Technology/Albanora, SE-106 91 Stockholm, Sweden.

 © 2004 American Institute of Physics

Downloaded 27 Dec 2004 to 130.237.35.30. Redistribution subject to AIP license or copyright, see http://rsi.aip.org/rsi/copyright.jsp

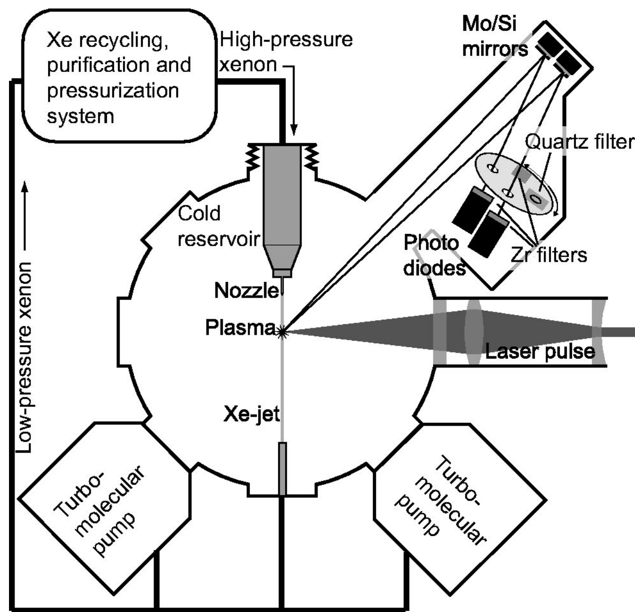

FIG. 1. The general experimental arrangement for liquid-xenon-jet laser-plasma generation and EUV-in-band-emission monitoring.

measurement techniques have been developed for many of the characterization experiments. The results are discussed in relation to the full-system requirements.

II. GENERAL EXPERIMENTAL ARRANGEMENT AND EUV PERFORMANCE

The general experimental arrangement for laser-plasma generation using a liquid-xenon-jet as target is illustrated in Fig. 1. The liquid-jet is formed by forcing xenon gas under high pressure into a reservoir cooled to liquefy the xenon. A tapered glass capillary nozzle with an orifice diameter of typically 10–30 μm is attached to the reservoir, producing a microscopic liquid jet into an ultra-high-vacuum compatible chamber. Vacuum is maintained by two ~2000 l/s turbomolecular pumps resulting in pressures of $10^{-4}-10^{-3}$ mbar during operation. The base pressure of the system before operation is typically in the $10^{-8}-10^{-7}$ mbar range but could be further reduced through, e.g., baking of the system. To reduce the load on the turbomolecular pumps during operation, the nonevaporated part of the xenon jet is extracted from the chamber through a differential-pumping scheme. The xenon evacuated through both the turbomolecular pumps and the jet-extraction system is further collected by a recycling, purification, and pressurization system allowing for closed-loop usage of xenon, considerably reducing the cost of operation. The plasma is generated by focusing Nd:YAG-laser pulses of $\lambda=1064$ nm, ~5 ns pulse length, and up to 350 mJ pulse energy onto the jet through a focussing system theoretically capable of obtaining a full width at half maximum (FWHM) ~10 μm spot. The EUV emission is monitored by a flying-circus tool[16] (FCII) further described in Ref. 17. The best conversion efficiency (CE) of laser energy to in-band EUV emission obtained is 0.95%/(2% BW 2πsr) at $\lambda=13.45$ nm.

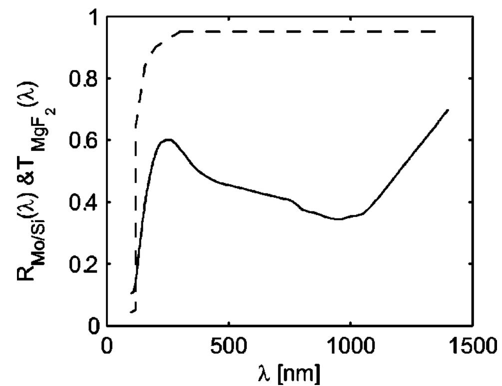

FIG. 2. The reflectivity of a Mo/Si mirror (solid line) and the transmission of a MgF_2 filter (dashed line).

III. OUT-OF-BAND RADIATION

Unfortunately the xenon plasma emits radiation also outside the desired ~2% bandwidth around $\lambda\sim13.5$ nm that is transmitted by the optical system of an EUVL stepper based on Mo/Si multilayer mirrors. This out-of-band radiation will have a negative impact on EUVL system performance. The broad-band soft-x-ray and EUV radiation may induce carbon growth and oxidation on mirror surfaces.[18] However, this out-of-band short-wavelength radiation will not be transmitted through the full system since it is effectively absorbed in the first near-normal-incidence multilayer mirror it encounters. This will, though, lead to heating of this mirror. For longer wavelengths, $\lambda>120$ nm, the Mo/Si mirrors reflect radiation[19] as is illustrated in Fig. 2. This DUV radiation is especially harmful since it can expose the resist if it reaches the wafer.[19] Furthermore, all radiation that is transmitted through the optical system will increase the thermal load on components throughout the system. In this section we will mainly treat the DUV radiation. System studies indicate that the maximum acceptable level of DUV radiation in the $\lambda>130-400$ nm range into the secondary focus after the collector mirror is $\leq7\%$ of the total radiation into 2% bandwidth around 13.5 nm.[15] Operation above this level will probably require a spectral purity filter which also will attenuate the in-band EUV radiation, leading to a higher demand on total power from the source. In order to estimate the wavelength dependent emission into 2π steradian $E(\lambda)$ of the plasma, two experiments were performed.

First, the DUV radiation was measured using the FCII tool discussed above as illustrated in Fig. 3(a). One photodiode was, in this case, equipped with an MgF_2 filter transmitting wavelengths $\lambda>120$ nm (see Fig. 2) to block in-band EUV radiation reflected by the Mo/Si mirror. The other photo diode was covered by a 200 nm thick zirconium filter to measure in-band EUV as a reference. The filter wheel was equipped with an optical filter, transmitting wavelengths $\lambda>400$ nm, that could be inserted in front of the MgF_2 filter. By subtracting the signal from measurements with both the MgF_2 and the $\lambda>400$ nm filter from measurements with only the MgF_2 filter, the signal from only the $\lambda>120-400$ nm wavelength range could theoretically be determined. However, in the present measurement the $\lambda>400$ nm signal was below the detection limit due to a high background-noise

Downloaded 27 Dec 2004 to 130.237.35.30. Redistribution subject to AIP license or copyright, see http://rsi.aip.org/rsi/copyright.jsp

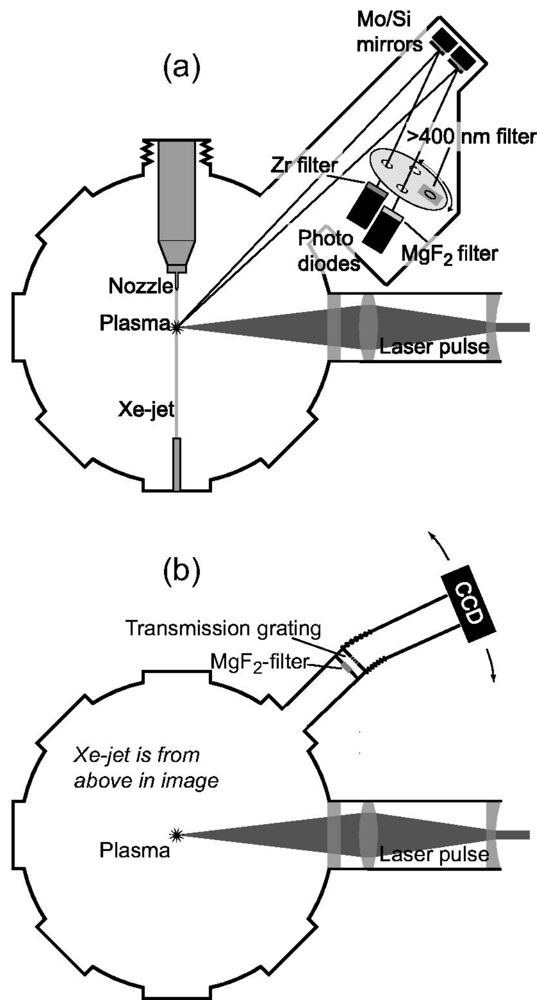

FIG. 3. The experimental arrangements for out-of-band-energy measurement with the flying-circus tool (a) and out-of-band spectroscopy (b).

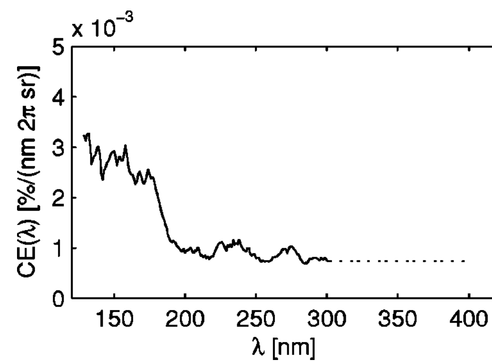

FIG. 4. The wavelength-dependent conversion efficiency of laser energy to broadband DUV emission. The dotted line illustrates extrapolated data.

level, not allowing for this subtraction. Instead, it was assumed that the out-of-band signal obtained with only the MgF_2 filter was due only to radiation in the $\lambda>120-400$ nm wavelength range. The scattered-light background was determined by tilting the corresponding mirror to focus the radiation outside the photodiode surface.

The detected signal of the photo diode, Q_d, is given by

$$Q_d=\int_\lambda E(\lambda)T_{\mathrm{MgF_2}}(\lambda)R_{\mathrm{Mo/Si}}(\lambda)\,\eta_d(\lambda)\,\frac{\Omega}{2\pi}\,d\lambda, \tag{1}$$

where $T_{\mathrm{MgF_2}}(\lambda)$, $R_{\mathrm{Mo/Si}}(\lambda)$, and $\eta_d(\lambda)$ are the wavelength dependent transmission of the MgF_2-filter, reflectivity of the Mo/Si-mirror, and quantum efficiency of the photodiode, respectively. Ω is the solid angle collected by the Mo/Si-mirror.

Since it is not possible to determine $E(\lambda)$ from only Eq. (1), the DUV spectrum ($\lambda<300$ nm) was obtained using a spectrographic arrangement as illustrated in Fig. 3(b), noting that the spectrograph is not oriented in the direction of FCII which might introduce an error. This is built up of a 1000 lines/mm free-standing transmission grating (Heidenhein GmBH) in combination with a cooled, thinned, back-illuminated 1024×1024 pixel charge-coupled device (CCD) array (Andor DO434) with normalized spectral response $\eta_{\mathrm{CCD}}(\lambda)$. A MgF_2 filter with transmission $T_{\mathrm{MgF_2}}(\lambda)$ was used to filter out higher-order components of shorter wavelengths. The detected signal on the CCD is $I_{\mathrm{CCD}}(\lambda)$ and the wavelength dependent emission per pulse of the plasma is in this case given by

$$E(\lambda)=C\,\frac{I_{\mathrm{CCD}}(\lambda)}{T_{\mathrm{MgF_2}}(\lambda)\,\eta_{\mathrm{CCD}}(\lambda)}, \tag{2}$$

where C is a constant containing the absolute efficiency of the spectrograph and the constant of the efficiency of the CCD. C is unknown, but can be found by inserting the expression for $E(\lambda)$ from Eq. (2) into Eq. (1) and solving for C. Since only $\lambda<300$ nm was registered with the spectrograph, the spectra is extrapolated to $\lambda=400$ nm with the value at $\lambda=300$ nm. Furthermore, the calculation assumes, as previously mentioned, that all DUV out-of-band radiation is emitted within $\lambda<400$ nm, which will lead to a worst-case over-estimation of this radiation.

By inserting this expression for C into Eq. (2) the absolute emission per pulse $E(\lambda)$ is obtained. By further dividing $E(\lambda)$ with the laser pulse energy, the wavelength-dependent out-of-band conversion efficiency CE(λ) is obtained as illustrated in Fig. 4. Finally, the total conversion efficiency into $\lambda=120-400$ nm and 2π steradian $\mathrm{CE_{DUV}}$ is found from

$$\mathrm{CE_{DUV}}=\int_{\lambda=120\ \mathrm{nm}}^{\lambda=400\ \mathrm{nm}}\mathrm{CE}(\lambda)\,d\lambda \tag{3}$$

and into the secondary focus, given a normal-incidence Mo/Si collector

$$\mathrm{CE_{DUV-2ndFoc}}=\int_{\lambda=120\ \mathrm{nm}}^{\lambda=400\ \mathrm{nm}}\mathrm{CE}(\lambda)R_{\mathrm{Mo/Si}}(\lambda)\,d\lambda. \tag{4}$$

The value obtained for $\mathrm{CE_{DUV}}$ is ~0.33% which should be compared to the in-band CE of ~0.55%/(2%BW 2πsr) at $\lambda=13.45$ nm that was simultaneously measured in the actual experiment. This gives a fraction of in-band EUV and out-of-band DUV from the source of 60%. $\mathrm{CE_{DUV-2ndFoc}}$ into the secondary focus is ~0.15% to be compared with 0.55%×70%=0.38% for in-band EUV given an in-band-EUV reflectivity of 70%. This gives a fraction of 39%, 5.6× higher than the required 7% mentioned above. The result is expected to be correct within a factor of two, where the main error is due to the uncertainty in the DUV spectral content.

Downloaded 27 Dec 2004 to 130.237.35.30. Redistribution subject to AIP license or copyright, see http://rsi.aip.org/rsi/copyright.jsp

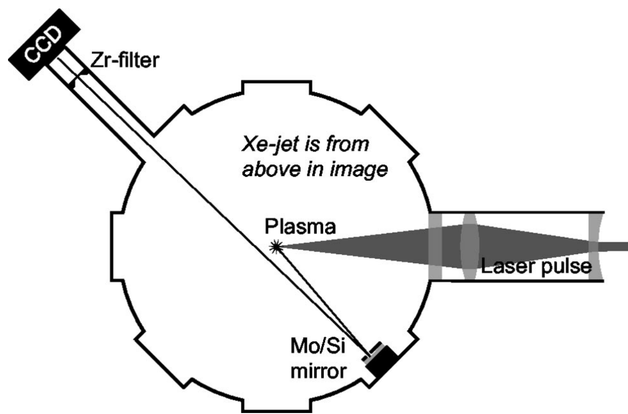

FIG. 5. The experimental arrangement for EUV in-band imaging based on a spherical Mo/Si mirror and a CCD detector.

Further experiments should use a spectrographic setup better adapted for absolute DUV measurements. One should also observe that no effort was made to optimize the experiment for low DUV emission. Furthermore, the measured DUV radiation is emitted by the full plasma. A significant fraction of the DUV radiation will be emitted by the colder wings of the expanding plasma although the actual size of the DUV emitting plasma has not yet been experimentally determined. However, spatial filtering of the hot EUV-emitting core should improve the EUV/DUV ratio. In combination with optimization for low DUV emission and more accurate diagnostics it is likely that the 7% DUV/EUV ratio can be met. This is supported by another xenon laser-plasma experiment showing a DUV/EUV ratio at the secondary focus of 4%.[20]

IV. SHAPE AND SIZE OF PLASMA

Knowledge of the size of the EUV-emitting plasma is important since, e.g., the étendue of the system will limit the collectable fraction of the energy radiated from the plasma.[21,22] The étendue is given by the emitting source area A and the numerical aperture, of the collector as[23]

$$\text{étendue} = A \times \pi \times \text{NA}^2. \tag{5}$$

At the same time, the emission profile is also an important input to the design of an illumination system of an EUV tool in order to achieve the desired illumination uniformity. The emission profile of plasmas have traditionally been imaged by pinhole cameras.[13] The main disadvantage is that this technique is not wavelength selective, and it has been shown that the EUV in-band image of a plasma might not correspond to a broadband image.[24] Moreover, it is difficult to obtain good spatial resolution using a pin-hole camera, which is especially important when imaging very small plasmas. A zone-plate-based camera can give very high resolution[25] but cannot be used here since it requires a monochromatic source due to the inherent chromatic aberrations of the diffractive optics. Instead an EUV camera based on a spherical multilayer mirror was developed to obtain both wavelength selectivity and high spatial resolution simultaneously.

The EUV camera arrangement is illustrated in Fig. 5. It consists of a spherical Mo/Si mirror, a Zr-filter to block visible radiation and a CCD detector. The mirror has a radius of curvature of 500 mm and a clear aperture of 10 mm. It is mounted 300 mm from the plasma on a tripod arrangement allowing for both tilt and translation. The CCD detector is mounted 1500 mm from the mirror, resulting in a 5× magnification. In order for the plasma not to interfere with the optical path, both the mirror and the CCD are mounted somewhat nonsymmetrically as illustrated in Fig. 5. This results in that the object (the plasma) is ~7 mm off-axis. Ray tracing was performed using the ZEMAX software, indicating that a resolution of 8 μm should be obtainable.

By focusing the laser as tightly as possible on the xenon-jet a very small plasma, ~20 μm FWHM, can be obtained as illustrated in Fig. 6(a). However, by defocusing the laser and changing the laser-pulse parameters the size of the plasma can also be increased. A 200–270 μm FWHM plasma is shown in Fig. 6(b).

A disadvantage with the very small plasma is that the CE is typically somewhat lower than normal, e.g., ~0.35%/(2%BW 2πsr) for the case of Fig. 6(a). However, in certain applications, this is well compensated by that the smaller source results in a very high brightness ($\text{W/m}^2\text{/sr}$). This is advantageous in applications with a small étendue (cf. Ref. 22). A larger source, having optimal CE, is better suited for a stepper. Even if the full geometrical diameter of the plasma is considered, $d \sim 400\,\mu\text{m}$, and a large collection angle of $2\pi\cdot\text{sr}$ (NA=1) the resulting étendue is ~0.4 mm^2 which is well below the presently estimated maximum allowable source output étendue[15] of 1–3.3 mm^2. Thus, no power from the laser-plasma source will be lost due to the étendue limitation. This is in contrast to the larger-diameter discharge sources where such loss may become important.[21]

V. REPETITION-RATE LIMIT

It is preferable to operate an EUV source at as high repetition rate as possible.[26] In that way, more pulses will be integrated in each exposure, improving the dose accuracy and, thus, the critical dimension control. The present thinking is that an EUV-stepper source should operate at >7–10 kHz.[15]

The limiting factor for the repetition rate of a liquid-xenon-jet laser-plasma source is the time after one plasma shot until new unaffected target material is available in the laser-focus point. The maximum repetition rate was previously estimated by investigating how large portion of the jet is affected by a single laser pulse.[27] That study estimated the maximum repetition rate to 30 kHz at a jet velocity of 50 m/s.

In order to further investigate the maximum repetition rate, high-repetition-rate operation was simulated in a double-pulse setup in which two plasmas were generated with a very short time separation. By varying the time-delay between the two pulses and investigating the shot-to-shot EUV stability from the second pulse, the minimum time delay before the first pulse affects the second pulse can be found. For a jet velocity of 60 m/s, Fig. 7 illustrates how a significant stability transition from 3.8% (1σ) to 36% was found when changing the delay from 60 to 50 μs, corre-

Downloaded 27 Dec 2004 to 130.237.35.30. Redistribution subject to AIP license or copyright, see http://rsi.aip.org/rsi/copyright.jsp

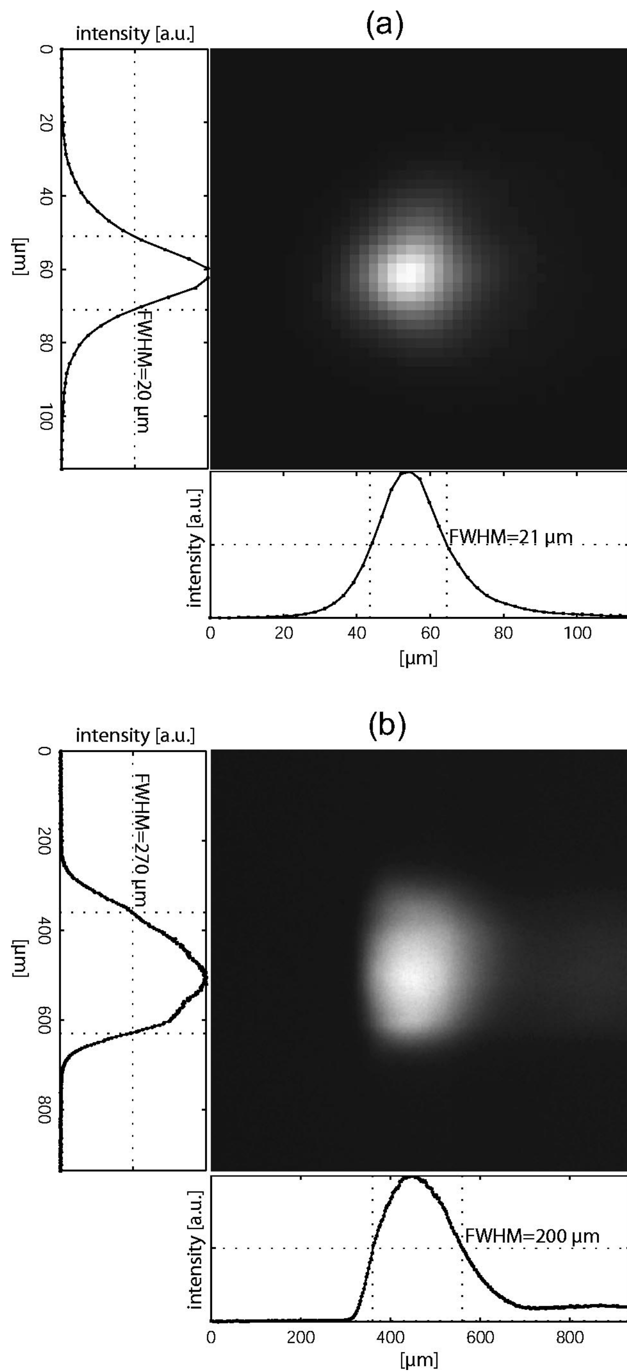

FIG. 6. Image of a small plasma (5 shots averaged) in (a) and larger plasma (40 shots averaged) in (b). The emission tail in the image (b) is an artifact due to that the CCD was read out during continuous exposure.

sponding to an increase in repetition rate from 17 to 20 kHz. At the shorter time separation, the second pulse is not always fired on an intact jet target but rather on the jet region that may be damaged by the first pulse. The experiment indicates that a liquid-xenon-jet laser-plasma source can be operated with a repetition rate of at least 17 kHz. Although it is below the result of the previous study of 30 kHz it is still well above the 7–10 kHz previously discussed. It should also be noted that an increase in jet velocity would allow for higher repetition rates.

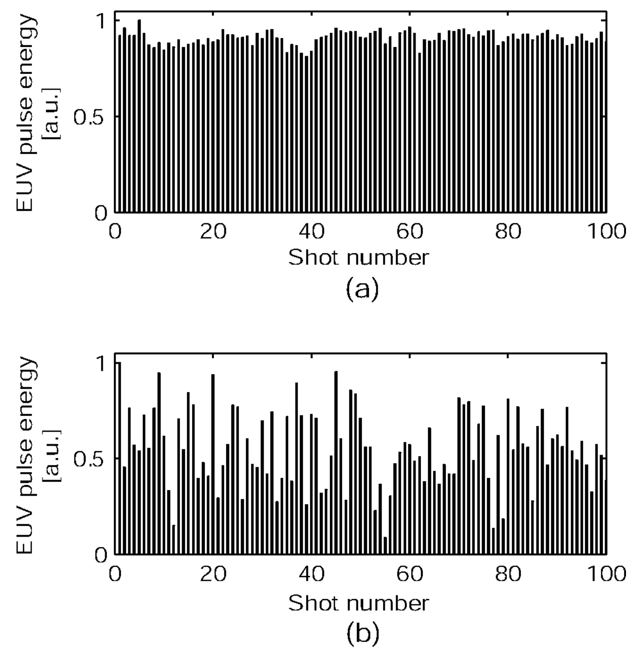

FIG. 7. For a jet velocity of 60 m/s two plasmas are generated with a small time separation. The pulse-to-pulse EUV stability of the second pulse is illustrated in the figure. In (a) the temporal delay is 60 μs corresponding to 17 kHz and in (b) 50 μs corresponding to 20 kHz. The 1 σ stability goes from 3.8% in (a) to 36% in (b).

VI. SPUTTERING BY ENERGETIC XENON IONS

Contamination and wear induced by the source on especially the collector mirror is one of the largest obstacles to overcome toward the realization of EUVL. Although the use of a xenon-liquid-jet laser-plasma source has several advantages, such as operation with a noble-gas target material, thereby avoiding condensation of target vapor on the collector,[14] and a large working distance from plasma to any source hardware,[27] there are still critical issues to solve. A major issue is sputtering by energetic xenon ions. As illustrated in Fig. 8 there are two sputtering issues. First, the energetic ions may directly sputter the surface of the collector, reducing its reflectivity. Furthermore, the ions may sputter other components in the vicinity of the plasma and in that way release material that may deposit on the collector mirror, also reducing its reflectivity. It is therefore important to un-

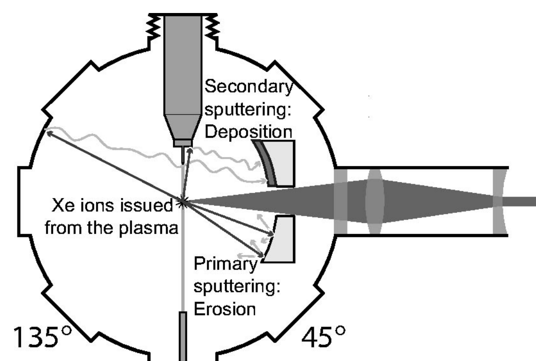

FIG. 8. Energetic xenon ions from the plasma can lead to both direct sputtering (primary) of the collector mirror and sputtering (secondary) of other material in the vicinity of the source releasing material that may deposit on the collector mirror.

Downloaded 27 Dec 2004 to 130.237.35.30. Redistribution subject to AIP license or copyright, see http://rsi.aip.org/rsi/copyright.jsp

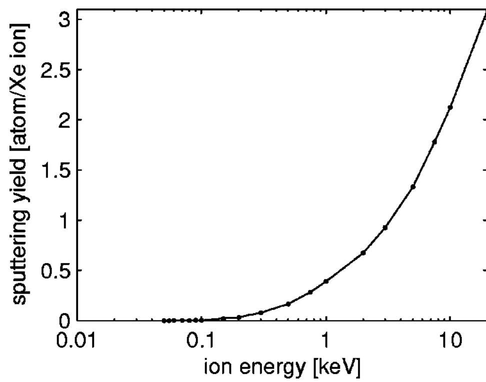

FIG. 9. The calculated sputtering yield of xenon ions on a Mo/Si mirror.

derstand both the ion emission characteristics of the xenon plasma and the energy-dependent sputter yield (number of knocked-out atoms per ion).

The sputter yield of xenon ions on a Mo/Si mirror was estimated using the SRIM 2000 software package.[28] As can be seen in Fig. 9, it is about unity for xenon ions in the kilo-electron-volt energy range. It should, however, be noted that highly charged ions can have much higher sputter yields.[29] A time-of-flight experiment with a Faraday cup as ion detector (cf. Ref. 30) was performed to estimate the energies of the emitted ions from the plasma. The Faraday cup was mounted in both 45° and 135° to the laser direction (see Fig. 8) at a distance $d = 113$ mm from the plasma. Each pulse resulted in a voltage response as illustrated in Fig. 10. The first peak, at t_0, is fully synchronized with the laser pulse and is used as a temporal reference. The longer, second, peak is assumed to be due to xenon ions. Since the higher-energy ions are more damaging, we performed a worst-case-analysis of the data. Therefore, the time t_1 is defined as the rising edge of the ion peak. The time of flight of the ions is

$$\Delta t = t_1 - t_0, \tag{6}$$

and the energy of the ions, E_{Xe}, is then obtained from

$$E_{\mathrm{Xe}} = \frac{1}{2} m_{\mathrm{Xe}} \left(\frac{d}{\Delta t} \right)^2, \tag{7}$$

where m_{Xe} is the mass of a xenon atom.

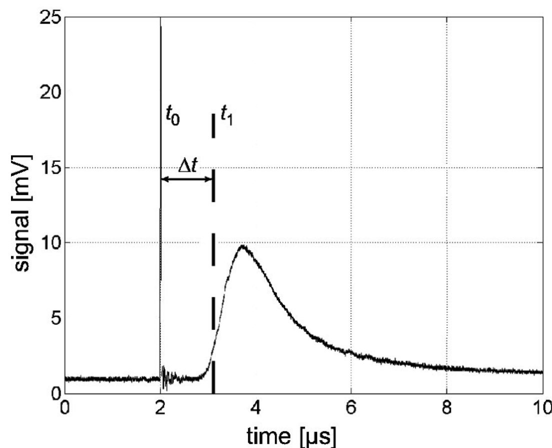

FIG. 10. The voltage response of the Faraday cup for a typical plasma event.

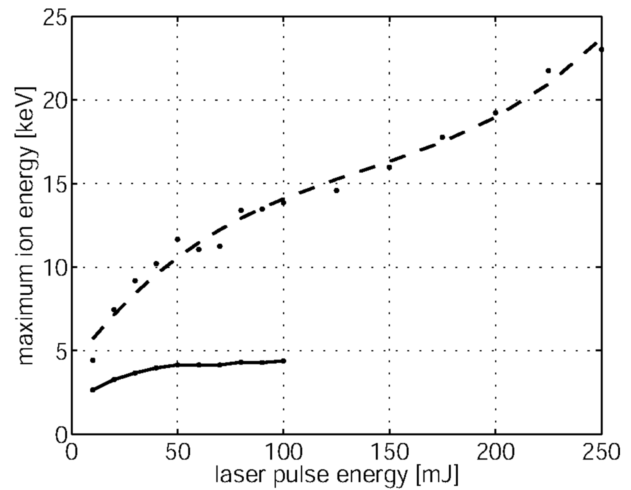

FIG. 11. The dependence of laser pulse energy on maximum ion energy. The dashed line was obtained with the Faraday cup in a 45° angle to the laser beam and the solid line in 135° (cf. Fig. 8).

The resulting maximum ion energies as a function of laser-pulse energy and direction of measurement is illustrated in Fig. 11. As can be seen, the peak energy of the ions is higher in the 45° direction than in the 135° direction. It should be noted that we also expect a long tail of lower-energy ions. However, this cannot be experimentally determined with the current arrangement since the signal is smeared out in time, resulting in a voltage response smaller than the measurement noise. Furthermore, quantitative ion flux numbers cannot be obtained since the average charge of the ions reaching the Faraday cup is not known. Future experiments should also try to determine the charge distribution of the ions due to the higher sputter yield expected from highly charged ions as mentioned above. The presence of multi-kilo-electron-volt xenon ions from plasmas created by several-nanosecond laser pulses is also reported in other studies of similar targets[20,31] and in solid-bulk-target.[30] Multi-kilo-electron-volt ions were, however, not found in a xenon-gas-puff target experiment.[30]

In order to verify the sputtering effect of the detected ions, silicon wafers were exposed to 10^6 plasma events generated by ~330 mJ laser pulses. The wafers were placed 110 mm from the plasma, both in the 45° and 135° directions (see Fig. 8). The wafers were masked except for a small area, and the edges between the masked and unmasked area were investigated with a surface profiler (KLA Tencor P-15) after the exposure. The unmasked area showed ~10 nm deep sputtering in the 45° direction and ~27 nm [see Fig. 12(a)] in the 135° direction.

This significant sputtering is expected given the highly energetic ions observed although no quantitative comparison can be made since the Faraday-cup measurements do not yield quantitative data regarding the number of ions. It is furthermore interesting to note that the sputtering rate is higher in the 135° direction although the maximum ion energies are higher in the 45° direction. This probably indicates a larger number of ions emitted in the 135° direction. These may be lower-energy ions that cannot be detected with the current Faraday-cup setup.

Downloaded 27 Dec 2004 to 130.237.35.30. Redistribution subject to AIP license or copyright, see http://rsi.aip.org/rsi/copyright.jsp

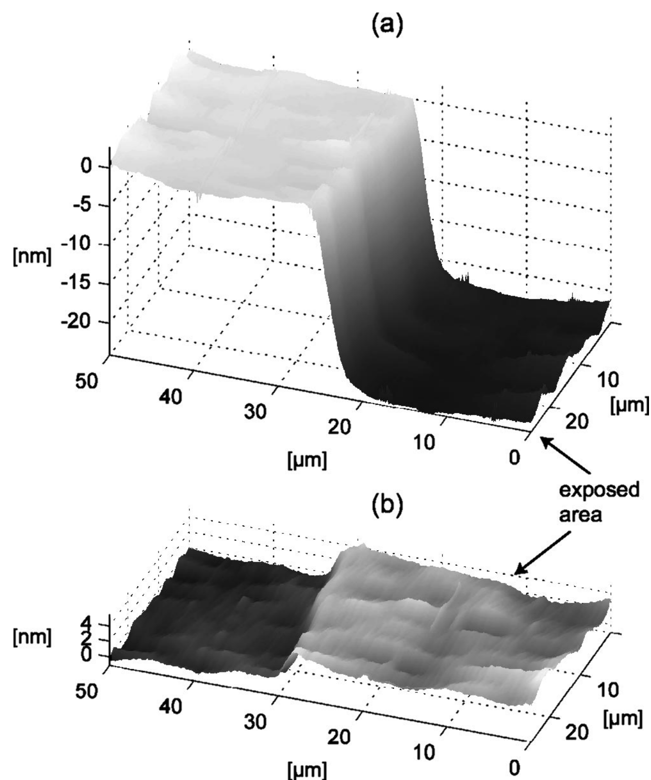

FIG. 12. Edge between masked and unmasked area of silicon wafer exposed to 10^6 plasma events in the 135° direction without increased background pressure (a) and in the 45° direction with increased background pressure (b). Sputtering is observed in (a) and an unidentified deposition in (b).

It has previously been reported that a background pressure can reduce the energy of the fast ions.[32,33] A simple experiment was therefore performed where the turbomolecular pumps were stopped, increasing the xenon pressure in the vacuum chamber to >1 mbar. Two more silicon wafers were then exposed under identical conditions. Indeed, no sputtering was observed, but rather a deposition of ~4 nm in both the 45° and the 135° direction [see Fig. 12(b)]. The composition of the deposition has, however, not been analyzed. Although the background pressure of >1 mbar is too high since it will absorb most of the in-band EUV radiation over a short distance, at least the concept is shown. Further experiments should be performed where the background pressure can be accurately controlled, and using other gases than the highly EUV-absorbing xenon. Other ion-mitigation methods such as electrostatic repeller fields[34] or magnetic-field shields[35] should also be investigated, although the high average ion energies will make the use of, at least, electrostatic repeller fields difficult.

VII. DISCUSSION

An EUV source has to meet demanding requirements to be suitable for EUVL systems. The present article has reported on the characterization of several vital parameters related to the source's applicability in a stepper. Although some parameters do not fully meet the required values, promising improvements are identified that may put the values within the requirements. The main issue to solve is believed to be the stopping of the highly energetic ions from the xenon plasma. If a means can be found to thermalize the ions and reduce their charge before they reach any component surface within the source, a liquid-xenon-jet laser plasma source could be a truly noncontaminating source. Especially the use of a background gas to decelerate the ions should therefore be studied further. However, this should be combined with efforts to lower the energies of the generated ions from the plasma.

ACKNOWLEDGMENTS

The authors would like to thank Caspar Bruineman of SCIENTEC Engineering for our joint development of the EUV plasma-imaging microscope, Heide Stollberg for the ZEMAX ray-tracing, and Anders Holmberg for the surface-profiler experiments.

[1] L. Rymell, M. Berglund, B. A. M. Hansson, and H. M. Hertz, Proc. SPIE **3676**, 421 (1999).
[2] B. A. M. Hansson, L. Rymell, M. Berglund, and H. M. Hertz, Microelectron. Eng. **53**, 667 (2000).
[3] J. E. Bjorkholm, Intel Tech. J. **Q3**, 1 (1998).
[4] *Next Generation Lithography (NGL) Workshop*, Pasadena, California, available at www.sematech.org (2001).
[5] K. Kemp, in *1st International EUV Lithography Symposium*, Dallas, Texas (2002), available at www.sematech.org.
[6] *EUVL Source Workshop*, Santa Clara, CA, 2 (2003), available at www.sematech.org.
[7] D. A. Tichenor *et al.*, Opt. Lett. **16**, 1557 (1991).
[8] L. Malmqvist, A. L. Bogdanov, L. Montelius, and H. Hertz, J. Vac. Sci. Technol. B **15**, 814 (1997).
[9] C. J. Gaeta *et al.*, Proc. SPIE **4688**, 818 (2002).
[10] M. Berglund, L. Rymell, M. Peuker, T. Wilhein, and H. M. Hertz, J. Microsc. **197**, 268 (2000).
[11] H. Kondo, T. Tomie, and H. Shimizu, Appl. Phys. Lett. **69**, 182 (1996).
[12] H. M. Hertz, L. Malmqvist, L. Rymell, and M. Berglund, *Method and Apparatus for Generating X-Ray or EUV Radiation* (1999), U.S. Patent No. 6,002,744.
[13] L. Malmqvist, L. Rymell, M. Berglund, and H. M. Hertz, Rev. Sci. Instrum. **67**, 4150 (1996).
[14] T. Mochizuki and C. Yamanaka, Proc. SPIE **733**, 23 (1987).
[15] H. Franken, Y. Watanabe, and K. Ota, presented at *EUVL Source Workshop in Antwerpen, Belgium*, 2003, www.sematech.org.
[16] R. Stuik, R. C. Constantinescu, P. Hegeman, J. Jonkers, H. F. Fledderus, V. Banine, and F. Bijkerk, Proc. SPIE **4146**, 121 (2000).
[17] B. A. M. Hansson, L. Rymell, M. Berglund, O. Hemberg, E. Janin, J. Thoresen, and H. M. Hertz, Proc. SPIE **4506**, 1 (2001).
[18] N. Koster *et al.*, Microelectron. Eng. **61–62**, 65 (2002), and references therein.
[19] J. Benschop, R. Gontin, V. Banine, and N. Harned, in *EUV Lithography Source Workshop*, Matsue, Japan (2001), available at www.sematech.org.
[20] *TRW/Cutting Edge Optronics Laser-Produced Plasma EUV Source Program*, EUV Source Workshop, Dallas, Texas (2002), available at www.sematech.org.
[21] G. H. Derra and W. Singer, Proc. SPIE **5037**, 728 (2003).
[22] B. A. M. Hansson, S. Mosesson, and H. M. Hertz (unpublished).
[23] M. Antoni, W. Singer, J. Schultz, J. Wangler, I. Escudero-Sanz, and B. Kruizinga, Proc. SPIE **4146**, 25 (2000).
[24] I. V. Fomenkov, R. M. Ness, I. R. Oliver, S. T. Melnychuk, O. V. Khodykin, N. R. Bowering, C. L. Rettig, and J. R. Hoffman, Proc. SPIE **5037**, 807 (2003).
[25] R. Fruke, T. Wilhein, M. Wieland, and U. Vogt, J. Phys. IV **104**, 153 (2003).
[26] V. Banine, J. P. Benschop, M. Leenders, and R. Moors, Proc. SPIE **3997**, 126 (2000).
[27] B. A. M. Hansson, R. Lars, M. Berglund, O. E. Hemberg, E. Janin, J. Thoresen, S. Mosesson, J. Wallin, and H. M. Hertz, Proc. SPIE **4688**, 102 (2002).
[28] J. F. Ziegler, SRIM 2000, software available at www.srim.org.

Downloaded 27 Dec 2004 to 130.237.35.30. Redistribution subject to AIP license or copyright, see http://rsi.aip.org/rsi/copyright.jsp

[29] J. D. Gillaspy, L. Ratliff, J. Pomeroy, and S. Bajt, *Study of EUV Source Collector Damage Mechanism* (2003), CD-ROM proceedings from 2nd Intenational EUVL Symposium in Antwerpen, Belgium, available from www.sematech.org.
[30] H. Daido, S. Yamagami, M. Suzuki, H. Azuma, I. W. Choi, and H. Fiedorowicz, Appl. Phys. B: Lasers Opt. **71**, 385 (2001).
[31] A. Endo, presented at *EUVL Source Workshop in Antwerpen, Belgium*, 2003. Available at www.sematech.org.
[32] M. L. Ginter and T. J. McIlrath, Appl. Opt. **27**, 885 (1988).
[33] L. Shmaenok *et al.*, Microelectron. Eng. **23**, 211 (1994).
[34] K. Takenoshita, C.-S. Koay, M. C. Richardson, and I. C. E. Turcu, Proc. SPIE **5037**, 792 (2003).
[35] G. Niimi, Y. Ueno, K. Nishigori, T. Aota, H. Yashiro, and T. Tomie, Proc. SPIE **5037**, 370 (2003).

Downloaded 27 Dec 2004 to 130.237.35.30. Redistribution subject to AIP license or copyright, see http://rsi.aip.org/rsi/copyright.jsp